

Chemical Science

Accepted Manuscript



This is an *Accepted Manuscript*, which has been through the Royal Society of Chemistry peer review process and has been accepted for publication.

Accepted Manuscripts are published online shortly after acceptance, before technical editing, formatting and proof reading. Using this free service, authors can make their results available to the community, in citable form, before we publish the edited article. We will replace this *Accepted Manuscript* with the edited and formatted *Advance Article* as soon as it is available.

You can find more information about *Accepted Manuscripts* in the [Information for Authors](#).

Please note that technical editing may introduce minor changes to the text and/or graphics, which may alter content. The journal's standard [Terms & Conditions](#) and the [Ethical guidelines](#) still apply. In no event shall the Royal Society of Chemistry be held responsible for any errors or omissions in this *Accepted Manuscript* or any consequences arising from the use of any information it contains.



Chemical Science

ARTICLE

Framboidal ABC Triblock Copolymer Vesicles: A New Class of Efficient Pickering Emulsifier

C. J. Mable, N. J. Warren, K. L. Thompson, O. O. Mykhaylyk* and S. P. Armes*

Received 00th January 20xx,
Accepted 00th January 20xx

DOI: 10.1039/x0xx00000x

www.rsc.org/

Pickering emulsions offer important advantages over conventional surfactant-stabilized emulsions, including enhanced long-term stability, more reproducible formulations and reduced foaming problems. The recent development of polymerization-induced self-assembly (PISA) offers considerable scope for the design of a wide range of block copolymer nanoparticles with tunable surface wettability that may serve as bespoke Pickering emulsifiers. In the present study, we exploit PISA to design a series of model framboidal ABC triblock copolymer vesicles with exquisite control over surface roughness. Transmission electron microscopy (TEM) and small-angle X-ray scattering (SAXS) were utilized to characterize these nanoparticles, which were subsequently used to stabilize *n*-dodecane emulsion droplets in water. The adsorption efficiency, A_{eff} , of the nanoparticles at the *n*-dodecane/water interface was determined as a function of increasing vesicle surface roughness using a turbidimetry assay. A strong correlation between surface roughness and A_{eff} was observed, with A_{eff} increasing from 36 % up to 94 %. This is a significant improvement in Pickering emulsifier efficiency compared to that reported previously for similar vesicles with smooth surfaces. In summary, nanoparticles with appreciable surface roughness are much more effective Pickering emulsifiers and this parameter can be readily fine-tuned using a highly efficient PISA formulation.

Introduction

Pickering emulsions are water or oil droplets that are stabilized by colloidal particles and have been recognised for more than a century.¹ These systems typically exhibit greater droplet stability compared to surfactant-stabilized emulsions². This is the result of strong, essentially irreversible particle adsorption at the oil-water interface, which minimizes the interfacial area between the two immiscible liquids and provides a steric barrier towards droplet coalescence.^{2, 3} A wide range of nanoparticles such as silica sols^{4,5} polystyrene latexes⁶⁻⁹ and inorganic clays¹⁰ have been shown to be effective Pickering emulsifiers. More recently, cross-linked block copolymer nanoparticles prepared by reversible addition-fragmentation chain transfer (RAFT) polymerization^{11, 12} have proven to be effective oil-in-water¹³ and water-in-oil¹⁴ Pickering emulsifiers. For example, Thompson *et al.*¹³ prepared highly stable emulsions using poly (glycerol monomethacrylate-*block*-2-hydroxypropyl methacrylate-*block*-ethylene glycol

dimethacrylate) (PGMA-*b*-PHPMA-*b*-PEGDMA) triblock copolymer vesicles. Turbidimetry studies indicated that these nanoparticles had an adsorption efficiency of as low as 57 %, depending on the vesicle concentration used for homogenization. This relatively poor adsorption efficiency was in part attributed to the high water content of the vesicles, which leads to a low Hamaker constant compared to solid particles.

In principle, particle wettability can be modulated by increasing surface roughness in order to enhance interfacial adsorption and hence Pickering emulsion stability. This hypothesis has been recently verified by San-Miguel and Behrens, who coated cationic silica microparticles with anionic nanoparticles prepared from a commercial methacrylic acid/methyl methacrylate statistical copolymer (Eudragit S-100; 33 % methacrylic acid). Solvent annealing of the nanoparticle coating was used to control the surface roughness of the microparticles, which were subsequently utilized to prepare oil-in-water Pickering emulsions at pH 5.¹⁵ In a related study, carbon black particles possessing a characteristic fractal morphology were used to stabilize the water/*n*-octane interface.¹⁶

In the present study, we prepare a series of ABC triblock copolymer vesicles of exquisitely tunable surface roughness via RAFT aqueous dispersion polymerization.¹⁷ First, a poly(glycerol monomethacrylate) (PGMA) macromolecular chain transfer agent (macro-CTA) is chain-extended using 2-

Department of Chemistry, University of Sheffield, Brook Hill, Sheffield, South Yorkshire, S3 7HF.

Electronic Supplementary Information (ESI) available: [Details of the structural model used for SAXS analysis, DMF GPC traces, assigned ¹H NMR spectra, SAXS data and fittings in aqueous sucrose solution, schematic for three-layer model for SAXS analysis, SEM images of Pickering emulsions, visible absorption spectra and calibration plots for G₆₃H₃₅₀B₃ vesicles and two tables summarizing SAXS fitting parameters]. See DOI: 10.1039/x0xx00000x

hydroxypropyl methacrylate (HPMA) in aqueous solution. In situ polymerization-induced self-assembly (PISA) occurs to form nascent nanoparticles comprising poly(2-hydroxypropyl methacrylate) (PHPMA) cores that are sterically stabilized by the water-soluble PGMA chains.^{18–21} Depending on the relative volume fractions of the PGMA and PHPMA blocks, well-defined copolymer spheres, worms or vesicles can be obtained at relatively high solids directly in aqueous solution.²² The mechanism of formation of the vesicular morphology has been investigated by Blanazs et al.^{22, 23} Chambon and co-workers reported that chain extension of such PGMA-PHPMA precursor vesicles using a water-insoluble monomer such as benzyl methacrylate (BzMA) results in the formation of framboidal (raspberry-like) ABC triblock copolymer vesicles via seeded RAFT emulsion polymerization.²⁴ Herein, we revisit this formulation in order to gradually increase the target degree of polymerization (DP) of the PBzMA block over a wide range using the same batch of PGMA-PHPMA diblock copolymer vesicles. This systematic approach enables the evolution of the framboidal morphology to be explored in detail: a series of vesicles with gradually increasing surface roughness are produced, as judged by transmission electron microscopy (TEM) and small-angle x-ray scattering (SAXS). These framboidal vesicles are then employed to prepare oil-in-water Pickering emulsions using either *n*-dodecane or *n*-hexane as the droplet phase. The emulsions are characterized in terms of their droplet size distributions and the particle adsorption efficiency at the oil/water interface is assessed as a function of surface roughness. For the sake of brevity, a shorthand notation is utilized throughout the manuscript to describe the various block copolymers. Thus G, H, B, and E denote glycerol monomethacrylate, 2-hydroxypropyl methacrylate, benzyl methacrylate and ethylene glycol dimethacrylate, respectively. For example, $G_xH_yB_z$ represents a poly(glycerol monomethacrylate-block-2-hydroxypropyl methacrylate-block-benzyl methacrylate) copolymer, where *x*, *y*, and *z* indicate the mean degrees of polymerization (DP) of the three respective blocks.

Results and discussion

Synthesis and characterization

The initial RAFT solution polymerization of GMA was conducted in ethanol at 70 °C to generate a near-monodisperse G_{63} macro-CTA ($M_w/M_n = 1.16$; see Figure S1 and Table 1). After purification, this water-soluble macro-CTA was utilized for the *in situ* RAFT aqueous dispersion polymerization of HPMA at 15 % w/w solids. ¹H NMR studies indicated that >99% HPMA conversion was achieved within 2 h at 70 °C, as expected from previous studies.²³ Gel permeation chromatography (GPC) studies indicated that near-monodisperse diblock copolymers were obtained with minimal macro-CTA contamination and high blocking efficiencies ($M_w/M_n = 1.16$; see Figure S1 and Table 1). GPC traces were invariably unimodal but typically exhibited a high molecular weight shoulder. The latter feature is attributable to low levels

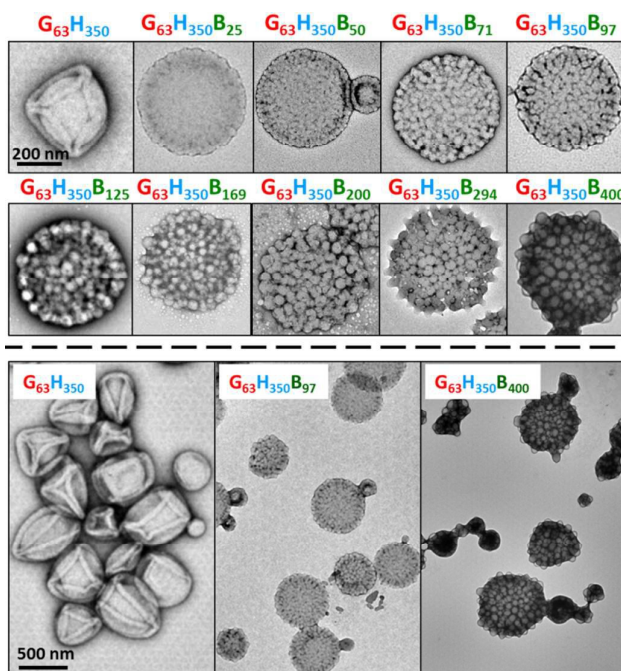


Fig. 1. Representative TEM images obtained for a series of framboidal $G_{63}H_{350}B_z$ triblock copolymer vesicles (where $z = 25-400$) and also the precursor $G_{63}H_{350}$ diblock copolymer vesicles. A 200 nm scale bar applies for the first ten images, while a 500 nm scale bar applies for the last three images.

of dimethacrylate impurity within HPMA (approximately 0.07 mol % as judged by HPLC analysis), which results in light branching of the PHPMA chains. TEM images (see first TEM image shown in Figure 1) reveal a pure vesicular morphology, as expected for this asymmetric diblock composition. The vesicle folds that are discernible in the TEM images are the result of buckling and/or partial collapse of these relatively delicate nano-structures under the ultrahigh vacuum conditions. These well-defined $G_{63}H_{350}$ diblock copolymer precursor vesicles were also characterized by DLS (see Table 1) and then utilized for the *in situ* RAFT seeded emulsion polymerization of BzMA at 70 °C to produce a series of nine $G_{63}H_{350}B_z$ triblock copolymers (where *z* ranges from 25 to 400). ¹H NMR studies for these triblock copolymers (see Figure S2) indicate conversions greater than 96 % (see Table 1). Signal *j* at 7.1–7.4 ppm, which is assigned to the five aromatic BzMA protons, increases on targeting higher DPs. DMF GPC studies confirmed that near-monodisperse triblock copolymers were obtained (M_w/M_n ranges from 1.10 to 1.25) with high blocking efficiencies; see Figure S1 and Table 1. It is noteworthy that these polydispersities are significantly lower than those reported by Chambon et al., who reported M_w/M_n values as high as 1.50.²⁴ This is most likely attributable to the higher macro-CTA/initiator molar ratio of 5.0 employed in the present work. In contrast, Chambon et al. used a macro-CTA/initiator molar ratio of just 2.0, which is known to lead to reduced living character for RAFT polymerizations and may also lead to homopolymer impurities.²⁵ Moreover, it is worth noting that Chambon et al. only targeted three $G_{58}H_{350}B_z$ copolymers, for which *z* was 200, 300 or 400.²⁴

Table 1. Summary of ^1H NMR calculated composition and conversion, GPC number-average molecular weight (M_n) and polydispersity (M_w/M_n) and DLS hydrodynamic diameter (D_h) obtained for a G_{63} macro-CTA, linear $G_{63}H_{350}$ diblock copolymer precursor vesicles and framboidal $G_{63}H_{350}B_z$ triblock copolymer vesicles (where z ranges from 25 to 400).

Copolymer Composition	Conv. (%)	M_n (kg mol^{-1})	M_w/M_n	D_h (PDI) (nm)
G_{63}	-	17.6	1.16	-
$G_{63}H_{350}$	>99 ^a	82.2	1.16	362 (0.08)
$G_{63}H_{350}B_{25}$	100	87.3	1.16	401 (0.09)
$G_{63}H_{350}B_{50}$	100	100.0	1.10	411 (0.09)
$G_{63}H_{350}B_{71}$	94	102.1	1.10	406 (0.09)
$G_{63}H_{350}B_{97}$	97	104.5	1.11	407 (0.07)
$G_{63}H_{350}B_{125}$	100	112.2	1.12	394 (0.04)
$G_{63}H_{350}B_{169}$	97	114.3	1.13	364 (0.06)
$G_{63}H_{350}B_{200}$	100	117.7	1.15	375 (0.08)
$G_{63}H_{350}B_{294}$	98	130.7	1.18	366 (0.05)
$G_{63}H_{350}B_{400}$	100	140.9	1.25	418 (0.12)

a. Refers to HPMA conversion in this case.

In the present study, we explore the evolution of the framboidal morphology in much more detail (nine $G_{63}H_{350}B_z$ copolymers, with z ranging from 25 to 400) while achieving significantly better control over the copolymer molecular weight distribution.

DLS and TEM studies indicate that the vesicle diameter is more or less unchanged as the PBzMA DP is increased (see Table 1 and Figure 1). TEM analysis of the $G_{63}H_{350}$ diblock copolymer precursor vesicles indicates a relatively smooth and featureless surface morphology (see Figure 1). After chain extension with BzMA, the vesicle surface becomes increasingly rough until individual micelle-like globules of approximately 34 nm can be observed at a block copolymer composition of $G_{63}H_{350}B_{97}$. This suggests that nano-scale phase separation occurs within the vesicle walls during the polymerization of BzMA, as previously reported by Chambon *et al.*²⁴ As the target PBzMA DP is increased, the globules grow in size and prominence.

Small-angle X-ray scattering (SAXS) studies

SAXS is used to further characterize this *framboidal* vesicular morphology. TEM images (Figure 1) suggest three distinct particle morphologies: vesicles with smooth membranes (morphology 1), vesicles with pitted membranes (morphology 2) and vesicles with globular membranes (morphology 3) (see Figure 2a). The latter morphology is comparable to the polymer core-particulate silica shell particles reported by

Balmer and co-workers²⁶⁻²⁹ In this earlier work, Monte Carlo simulations were utilized to demonstrate²⁶ that the SAXS patterns obtained for such nanocomposite particles can be described by a two-population model represented by a superposition of two scattering signals originating from a core-shell spherical particle (population 1) and the small spherical silica particles that formed the shell (population 2).

A similar approach to SAXS analysis has been undertaken in the present study. Accordingly, population 1 represents the vesicles and population 2 describes the globules within the vesicle membrane (see Figure 2a, morphology 3 and supporting information for the SAXS fitting model, Equation S1 to Equation S10). Population 1 of the proposed two-population model corresponds to the initial morphology 1 (smooth vesicles) and is thus appropriate for SAXS analysis of the $G_{63}H_{350}$ diblock copolymer precursor. Morphology 1 is well described by the vesicle model (population 1 in Equation S1), which produced a reasonably good fit to the SAXS pattern over six orders of magnitude of X-ray scattering intensity (Figure 2b, Table S1, $G_{63}H_{350}$). The calculated vesicle radius, R_{out} , of 176 nm (Table S1) is consistent with both TEM observations (Figure 1) and DLS data (Table 1). The mean vesicle diameter is estimated to be 350 nm by TEM analysis, while DLS studies indicate a mean hydrodynamic vesicle diameter (D_h) of 362 nm with a relatively low polydispersity index (PDI) of 0.08. The radius of gyration (R_g) of the G_{63} corona block was determined to be 2.1 nm from model fitting of the $G_{63}H_{350}$ SAXS pattern. This experimental value is comparable to a theoretical estimate: the projected contour length of a single GMA monomer is 0.255 nm (two carbon bonds in all-trans conformation), the total contour length of a G_{63} block, $L_{\text{PGMA}} = 63 \times 0.255 \text{ nm} = 16.07 \text{ nm}$ and the Kuhn length of 1.53 nm, based on the literature value for poly(methyl methacrylate)³⁰, result in an estimated R_g of $(16.07 \times 1.53/6)^{1/2}$, or 2.02 nm. The water volume fraction, x_{sol} , in the membrane core is approximately 0.50 according to the SAXS data fit. The vesicle model (population 1) also produced a good fit to the experimental SAXS patterns corresponding to the triblock copolymer vesicles containing a relatively short PBzMA block corresponding to morphology 2 (Figure 2b and Table S1, samples $G_{63}H_{350}B_{25}$ and $G_{63}H_{350}B_{50}$). This result is consistent with TEM observations (Figure 1), which suggests that such copolymer compositions produce only surface-pitted vesicles that do not significantly affect their membrane structure. However, in order to produce satisfactory fits to SAXS patterns obtained for genuine *framboidal* vesicles prepared by targeting longer PBzMA blocks (e.g. $G_{63}H_{350}B_z$, $z = 97-400$) incorporation of population 2 (spherical micelles, which correspond to the micelle-like globules) into the model, Equation S1, was essential (Figure 2c, SAXS data corresponding to a continuous phase comprising pure water). A superposition of scattering signals from two populations (vesicles and spherical micelles) used in the model produces good fits to the SAXS data over a wide range of PBzMA block DPs (Figure 2b and Table S1).

It is assumed that both the R_g of the PGMA block and the water content within the hydrophobic vesicles membrane do

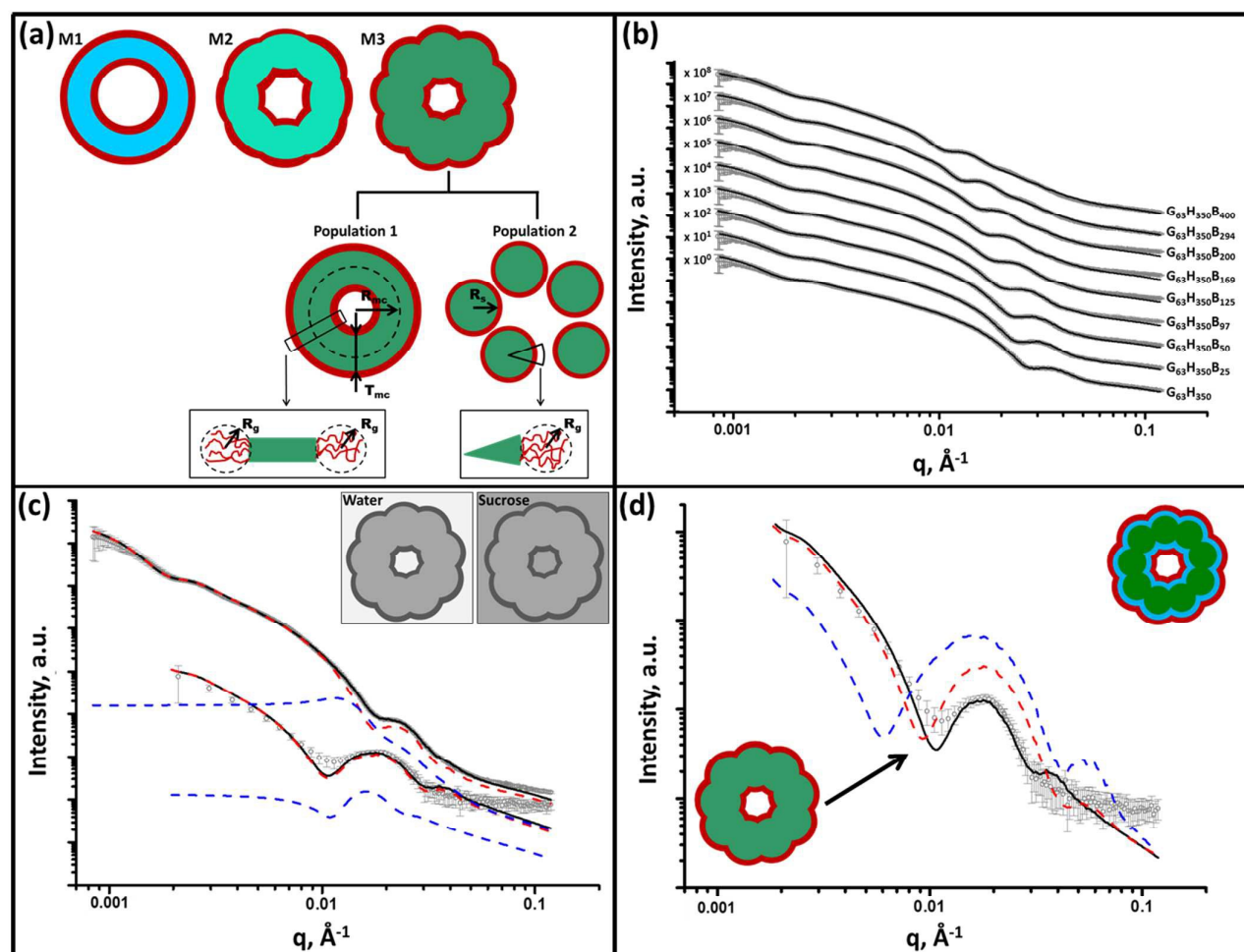


Fig. 2. Panel (a) shows a schematic representation of the structural morphology of both a $G_{63}H_{350}$ diblock copolymer precursor vesicle and a series of $G_{63}H_{350}B_z$ triblock copolymer vesicles, where red = PGMA (G), light blue = PHPMA (H), light green = mixed PHPMA and PBzMA (B) membrane where $z \leq 50$, and dark green = mixed PHPMA and PBzMA membrane where $z \geq 97$. Panel (b) shows SAXS patterns obtained for 1.0 % w/w aqueous dispersions of $G_{63}H_{350}$ diblock copolymer precursor vesicles ($z = 0$) and a series of framboidal $G_{63}H_{350}B_z$ triblock copolymer vesicles, where $z = 25, 50, 97, 125, 169, 200, 294$ or 400 . Solid lines represent fitting curves: For $z = 0, 25$ or 50 , a single population model was sufficient, whereas two populations were required for higher z values. For clarity, the SAXS patterns are shifted upward by an arbitrary factor indicated in the figure. Panel (c) displays SAXS patterns obtained for both 1.0 % w/w aqueous sucrose and aqueous dispersions of framboidal $G_{63}H_{350}B_{125}$ triblock copolymer vesicles. Fitting curves are represented by solid black lines. A two-population model was required for fitting [morphology 3 (M3) in panel (a)]: population 1 is represented by red dashed lines and population 2 is represented by blue dashed lines. Inset: schematic representations of the X-ray contrast achieved in both pure water and aqueous sucrose solutions. Panel (d) shows SAXS patterns obtained for a 1.0 % w/w aqueous sucrose dispersion of framboidal $G_{63}H_{350}B_{125}$ triblock copolymer vesicles. The solid black line represents the fit when a continuous core model was utilized and the dashed red line represents the fit when a fully phase-separated three-layer model was used for fitting. Inset: schematic representations of the continuous core model (left) and the phase-separated three-layer model (right).

not change during the growth of the PBzMA block. Thus, the R_g and x_{sol} values obtained for the $G_{63}H_{350}$ diblock precursor vesicles were used as fixed parameters for SAXS fitting of the final triblock copolymers. The same batch of PGMA macro-CTA was used for all copolymer syntheses described in this work, so the assumption of a fixed R_g for this block is perfectly reasonable. At first sight, it is questionable whether x_{sol} should remain constant when growing a progressively longer PBzMA block. This is because PBzMA is significantly more hydrophobic than PHPMA, hence a gradual reduction in x_{sol} with increasing PBzMA content might be expected. However, the developing framboidal character of the vesicle membrane necessarily leads to the incorporation of additional water

molecules (see Figure S3). We show below that this feature is sufficient to maintain a constant x_{sol} , regardless of the PBzMA content of the copolymer. An x_{sol} of 0.50 is obtained for the membrane-forming PHPMA block of the precursor $G_{63}H_{350}$ diblock copolymer vesicles. This value is consistent with recent work by Warren et al., who reported x_{sol} values ranging from 0.38 to 0.66 for $G_{55}H_y$ vesicles when varying y from 200 to 1000, respectively.³¹ Assuming additivity, if the PBzMA component has a water content of zero then x_{sol} might be expected to decrease from 0.50 for $G_{63}H_{350}$ diblock copolymer vesicles to 0.20 for $G_{63}H_{350}B_{400}$ triblock copolymer vesicles (see Table S2). Using these x_{sol} values as fitting parameters produces comparable results to those obtained when x_{sol} is kept constant at 0.50 (see Tables S1

and S2). This suggests that the SAXS parameters are relatively insensitive to x_{sol} . However, marginally better fits to the model, especially at high q , are obtained when x_{sol} is taken to be 0.50, regardless of the copolymer composition. This is most likely because, for population 1 of the SAXS model, it is assumed that water is distributed evenly within the hydrophobic component of the vesicle membrane (see Figure S3).

It is true that the overall volume fraction of water associated with the *hydrophobic* block(s) is *reduced* as the diblock copolymer precursor is chain-extended with BzMA. However, the local increase in curvature caused by the growth of the pseudo-spherical globules actually leads to a *higher* volume fraction of water becoming associated with the membrane *as a whole* (see yellow regions in Figure S3). This water volume fraction (or x_{sol}) can be estimated geometrically by calculating the free volume associated with a sphere of radius $0.5a$ placed within a cube of length a :

$$\frac{V_{\text{sphere}}}{V_{\text{cube}}} = \frac{1/6 \pi a^3}{a^3} = \frac{\pi}{6} \approx 0.50$$

SAXS analysis shows that the thickness of the hydrophobic component of the vesicle membrane (T_{mc}) increases on targeting higher DPs for the PBzMA block (Table S1 and Figure 3). However, the overall vesicle dimensions remain virtually constant over all copolymer compositions ($R_{\text{out}} \sim 174$ nm, Table S1), which is consistent with our TEM observations (Figure 1) and DLS studies (Table 1). Taken together, these data suggest that the vesicle growth mechanism leads to a gradual reduction in the volume of the vesicle lumen, as reported recently by Warren and co-workers for non-framboidal $G_{55}H_y$ vesicles, where y ranges from 200 to 2000.³² The nanoscale phase separation that occurs within the vesicle membrane described by the spherical micelle model (population 2) can also be identified from SAXS analysis.

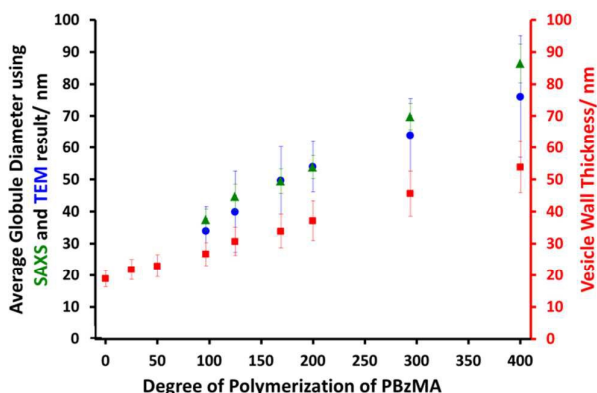


Fig. 3. Variation in mean micelle/globule diameter and vesicle wall thickness (T_{mc}) with degree of polymerization (z) for $G_{63}H_{350}B_z$ triblock copolymer vesicles obtained from SAXS (\blacktriangle , \blacksquare) and TEM (\bullet) data. [N.B. No mean globule diameters can be determined for $z = 0, 25$ and 50 because these vesicles do not exhibit framboidal character.]

Both the spherical micelle radius (R_s) and the relative concentration of the second population (c_2/c_1) increase at a higher PBzMA block volume fraction, V_{PBzMA} (Table S1). Moreover, the R_s values are consistent with those estimated from TEM images (Figure 3). TEM studies suggest that the mean micelle/globule diameter ($2R_s$) for the framboidal $G_{63}H_{350}B_z$ vesicles increases from 34 nm to 76 nm as z is increased from 97 to 400. Similarly, SAXS analyses indicate that $2R_s$ increases from 36 nm to 85 nm for the same set of samples. However, it is worth emphasizing that only a few hundred globules were analyzed by TEM, whereas the SAXS data are averaged over many millions of globules, which ensures far more robust statistics. Some difference between micelle/globule diameters measured by TEM and SAXS is likely because SAXS interrogates partially hydrated globules in aqueous solution. In contrast, TEM is performed on dehydrated globules under ultrahigh vacuum conditions, which accounts for the marginally smaller dimensions in this case. Moreover, SAXS reports a volume-average diameter whereas TEM provides a number-average diameter, hence the former technique always oversizes relative to the latter. The proposed structural model (Figure 2a) does not account for the nanoscale phase separation between the PHPMA and PBzMA blocks which might be expected to occur during PBzMA growth (see Figure 1). However, the difference between the scattering length densities of the copolymer components (ξ_{PGMA} , ξ_{PHPMA} and ξ_{PBzMA}) and water ($\xi_{\text{H}_2\text{O}}$) significantly exceeds the difference between the scattering length densities of the copolymer components alone (see Supporting Information for full details of the structural models used in the SAXS analysis). Thus SAXS is simply not particularly sensitive to the phase separation between the PHPMA and PBzMA blocks that is responsible for the evolution in morphology from smooth vesicles to framboidal vesicles during the PISA synthesis. Thus, in order to scrutinize the anticipated phase separation between the PHPMA and PBzMA blocks, a contrast variation technique was employed in this study. Accordingly, the vesicle dispersions were prepared using a 40 % w/w aqueous sucrose solution instead of water.

This solution is a good solvent for the PGMA stabilizer block and has a scattering length density of $\xi_{\text{H}_2\text{O}+\text{sucrose}} = 10.88 \times 10^{10} \text{ cm}^{-2}$, which lies between ξ_{PHPMA} and ξ_{PBzMA} (see Supporting Information). This contrast variation approach significantly reduces the scattering length density difference between the copolymer components and the continuous phase and consequently increases the sensitivity of SAXS towards the structural changes occurring within the vesicle membrane. It is emphasized that the PGMA stabilizer block has the highest scattering length density and hence produces a significant contribution to the scattering signal. Thus in principle contrast-matching the corona block ($\xi_{\text{PGMA}} = 11.94 \times 10^{10} \text{ cm}^{-2}$) to the solvent would be informative, but unfortunately this was not possible because of the limited solubility of sucrose in water.

The contrast-matched copolymer dispersions were prepared in two steps: (1) preparation of a 44 % w/w aqueous sucrose stock solution followed by (2) dilution of the copolymer dispersion prepared in pure water from 10 % w/w to 1 % w/w solids using this aqueous sucrose solution. The fitting parameters obtained for the purely aqueous dispersions were also used for SAXS analysis of the aqueous sucrose dispersions, while the solvent scattering length density used in the model was changed from that of water to that for 40 % w/w aqueous sucrose solution. Assuming that the vesicle morphology and the copolymer concentration remain unchanged in the aqueous sucrose dispersion, only six parameters are required for the SAXS fitting: the membrane thickness corresponding to the parameters used for population 1, the spherical micelle radius corresponding to population 2, their corresponding standard deviations and relative concentrations of both populations. For each sample, the concentration ratio, c_2/c_1 , was kept constant during the fitting at the same value obtained for the dispersions in pure water (Table S1). This relatively constrained model produced satisfactory data fits for the SAXS patterns of the aqueous sucrose dispersions (see Figure 2c, Figure S4 and Table S1). A significant inconsistency is only observed for the triblock copolymer prepared with the longest PBzMA block (Figure S4, see $G_{63}H_{350}B_{400}$). In this case, including additional fitting parameters in the model associated with the spherical micelle packing (R_{PY} and F_{PY}) and removing the c_2/c_1 ratio constraint produced a better data fit (Figure S4, solid red line). This latter fit indicated a significantly higher relative concentration for the second population (see the last entry in Table S1). This suggests that these nano-objects are best described as strongly interacting (i.e. aggregated) spherical micelles, with little or no vesicular character. In general, SAXS analysis of this series of vesicles dispersed in aqueous sucrose solution demonstrates that both the vesicle membrane thickness and the mean micelle radius are slightly reduced relative to the corresponding values determined for the same vesicles dispersed in pure water. The observed 15 vol % reduction in membrane volume (see Table S1) is the result of a lower degree of solvent plasticization. Presumably, this is simply because aqueous sucrose is a poorer solvent for the two blocks located in the membrane than water alone. Unfortunately, the relatively weak scattering from the aqueous sucrose dispersions means that SAXS pattern fits involving the other model parameters, including χ_{sol} , are considered unreliable. Nevertheless, the original SAXS model used for analysis of vesicle dispersions in pure water (Figure 2a) were consistent with the SAXS patterns recorded for dispersions in aqueous sucrose solution.

In order to probe the nanoscale phase separation between the PHPMA and PBzMA blocks within the vesicle membrane, a more sophisticated two-population model composed of vesicles with a three-layer hydrophobic membrane and spherical core-shell-corona micelles was developed (see Figure S5, Equation S1 and Equation S11 to

Equation S17). In this model, it is assumed that the PBzMA block occupies the central layer of the membrane. In principle, vesicles with the mean scattering length density of the hydrophobic component of the membrane that is closest to that of the aqueous sucrose solution (Table S1, see $G_{63}H_{350}B_{125}$ and $G_{63}H_{350}B_{169}$) should be most sensitive to nanoscale phase separation. If there is a homogeneous distribution of PHPMA and PBzMA blocks within the membrane (simple model, see Figure 2a), then the hydrophobic component of the membrane should barely contribute to the X-ray scattering as the difference between ξ_{mc} and $\xi_{H_2O+sucrose}$ is almost zero. Alternatively, if there is nanoscale phase separation between the PHPMA and PBzMA blocks (three-layer model, see Figure S5) the hydrophobic component of the membrane should produce a strong contribution to the scattering signal because of the significant difference between ξ_{PHPMA} and $\xi_{H_2O+sucrose}$ and between $\xi_{H_2O+sucrose}$ and ξ_{PBzMA} . Given that phase separation between the PHPMA and PBzMA blocks should cause a redistribution of solvent concentration within the vesicle membrane, two scenarios for the sophisticated two-population model (Equations S1, S11 and S14) were considered. As for the SAXS analyses summarized in Table S1, in one scenario it is assumed that the solvent fraction in the PBzMA layer and two PHPMA layers of the membrane are equal (i.e., $\chi_{PBzMA_{sol}} = \chi_{PHPMA_{sol}} = 0.50$). In an alternative scenario associated with Table S2, it is assumed that $\chi_{PBzMA_{sol}} = 0$ and $\chi_{PHPMA_{sol}} = 0.50$. Comparison of SAXS patterns calculated for the simple (single-layer) model and these two more sophisticated three-layer models indicates that the simple model is actually more consistent with the experimental data (Figure 2d).

To summarize the vesicle morphology studies, as the $G_{63}H_{350}$ diblock precursor is chain-extended with progressively longer PBzMA blocks, the overall vesicle diameter remains essentially constant (as indicated by DLS, TEM and SAXS) but the vesicle membrane thickness (as calculated by SAXS) increases. As a result, the vesicle lumen volume is gradually reduced on increasing the DP of the PBzMA. Finally, SAXS can be used to *quantify* the evolution in surface roughness indicated for these framboidal vesicles on the basis of TEM studies (see Figure 1). For $G_{63}H_{350}B_z$ triblock copolymer vesicles, both SAXS and TEM studies indicate that well-defined globules are only formed when $z > 97$ and the mean globule diameter increases monotonically from 36 nm ($z = 97$) to 85 nm ($z = 400$). However, a contrast variation approach used for SAXS analysis provides no evidence for the anticipated nanoscale phase separation between the hydrophobic PHPMA and PBzMA blocks within the membrane. This suggests that the PHPMA and PBzMA blocks may only be weakly segregated within the vesicle membrane, rather than strongly segregated (see Figure 2d).

Pickering emulsion studies

Framboidal $G_{63}H_{350}B_{200}$ triblock copolymer vesicles (an intermediate PBzMA block length) and linear $G_{63}H_{350}$ diblock copolymer vesicles were each evaluated as putative Pickering emulsifiers for the stabilization of *n*-dodecane emulsion droplets in water. Aqueous vesicle dispersions (0.5 to 3.0 % w/w) were homogenized with an equal volume of *n*-dodecane at 12,000 rpm for two minutes at 20 °C to produce Pickering emulsions. The concentration dependence of the mean droplet diameter of the resulting emulsions was determined by laser diffraction and optical microscopy (see Figure 4). Increasing the concentration of linear $G_{63}H_{350}$ vesicles led to a constant mean droplet diameter of $\sim 70 \mu\text{m}$. This suggests that the linear $G_{63}H_{350}$ vesicles do not withstand the high shear conditions required for emulsion preparation, and instead dissociate to produce individual copolymer chains, as previously reported by Thompson *et al.*^{13, 33} In contrast, the mean emulsion droplet diameter prepared using the $G_{63}H_{350}B_{200}$ triblock copolymer vesicles increases from 55 μm up to 412 μm over the same concentration range.

Similar concentration-dependent droplet diameters were observed for other $G_{63}H_{350}B_z$ copolymer vesicles. These observations suggest that the $G_{63}H_{350}B_z$ triblock copolymer vesicles survive high shear homogenization and consequently adsorb as intact triblock copolymer vesicles to produce genuine Pickering emulsions.

Remarkably, only a relatively short PBzMA block is required to stabilize the vesicles during homogenization; presumably, the highly hydrophobic nature of this third block is sufficient to prevent vesicle dissociation. TEM (see Figure 5a) and SEM studies (Figure S6) of the latter emulsions confirm that intact framboidal vesicles indeed act as Pickering emulsifiers. Hence the observed concentration dependence for the droplet diameter is readily explained: higher vesicle concentrations are required for stabilization of smaller oil droplets because of the concomitant increase in total surface area.

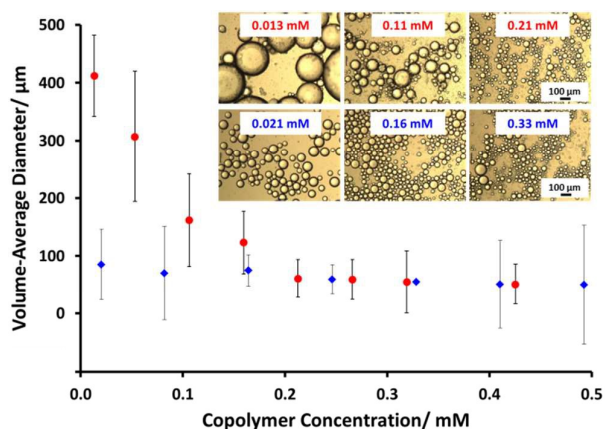


Fig. 4. Volume-average diameter (determined for *n*-dodecane droplets by laser diffraction) vs. copolymer concentration for (●) linear $G_{63}H_{350}$ diblock copolymer vesicles and (●) framboidal $G_{63}H_{350}B_{200}$ triblock copolymer vesicles. Inset shows representative optical microscopy images for selected emulsions prepared at the stated copolymer concentrations. The scale bars are valid for all six images.

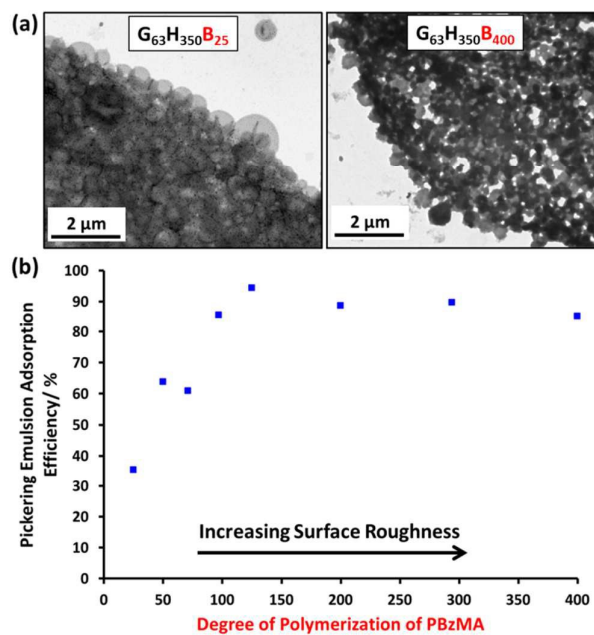


Fig. 5. (a) TEM images obtained for Pickering emulsions of *n*-hexane stabilized by aqueous vesicle dispersions of $G_{63}H_{350}B_{25}$ and $G_{63}H_{350}B_{400}$ triblock copolymer vesicles. (b) Plot of A_{eff} vs. PBzMA DP in a series of $G_{63}H_{350}B_z$ triblock copolymer vesicles (0.20 mM) with increasing surface roughness.

The Pickering emulsifier adsorption efficiency, A_{eff} , was determined by turbidimetry experiments, as described by Thompson *et al.*¹³ First, scattering curves were recorded and calibration plots were constructed for each triblock copolymer vesicle evaluated (see Figure S7). The scattering intensity increased monotonically as the PBzMA DP is increased in the $G_{63}H_{350}B_z$ triblock copolymer series, because of the significantly higher refractive index of this aromatic block. The Pickering emulsions proved to be highly stable towards coalescence, but creaming of the lower density droplet phase occurred on standing for 24 h at 20 °C. The turbidity of this lower aqueous phase was analyzed by visible absorption spectroscopy to determine the amount of vesicles remaining in the aqueous solution and hence the adsorbed amount by difference (see Table S3). To confirm the validity of this turbidimetric assay, the vesicles were also sized by DLS before and after homogenization in order to ensure that no size fractionation occurred during vesicle adsorption at the oil/water interface.

At a copolymer concentration of 0.20 mM, the A_{eff} increased from 36 % up to 94 % on increasing the PBzMA DPs from 25 to 125 (see Figure 5b). For PBzMA DPs greater than 125, the A_{eff} is progressively reduced, resulting in an A_{eff} of 85 % at a mean DP of 400 (see Figure 5b). These observations are similar to those reported by San-Miguel and Behrens,¹⁵ who observed that both the nanoparticle wettability and emulsion stability attained maximum values at the same root-mean-squared (rms) surface roughness. However, the latter parameter was calculated indirectly from AFM measurements performed on a planar surface that had been subjected to the same coating conditions as

the spherical microparticles. Nevertheless, it was suggested that wetting of microparticles with up to 6 nm rms roughness occurred within the Wenzel regime,³⁴ whereas the roughest microparticles (rms roughness = 7.5 nm) corresponded to the Cassie-Baxter regime.³⁵ The former regime led to optimal Pickering emulsifier performance. In the present study, the model *framboidal* vesicles exhibit substantially enhanced A_{eff} values compared to *non-framboidal* $G_{58}H_{350}E_{20}$ cross-linked vesicles, for which a A_{eff} of 67 % has been reported for a similar copolymer concentration.¹³ Presumably, the much higher surface roughness of the former nanoparticles (mean globule diameter \sim 45 nm) is responsible for this observation. This is significantly different to the critical length scale reported by San-Miguel and Behrens.¹⁵ However, it seems likely that other parameters, e.g. charge vs. steric stabilization or differences in copolymer composition, also influence the particle contact angle (and hence surface wettability).

Conclusions

$G_{63}H_{350}$ diblock copolymer precursor vesicles were chain-extended with BzMA via seeded RAFT emulsion polymerization at 70 °C to prepare a series of *framboidal* $G_{63}H_{350}B_z$ triblock copolymer vesicles (where z ranged from 25 to 400). TEM images reveal that the vesicle surface becomes increasingly pitted and rough until individual PBzMA globules can be observed protruding from the membrane. As higher PBzMA DPs are targeted, these globules gradually increase in size and become more prominent. SAXS provides a more in-depth analysis of surface roughness compared to TEM and DLS. Both SAXS and TEM studies confirm that topologically smooth vesicles are obtained prior to chain extension with BzMA, after which the vesicles acquire *framboidal* character (and hence surface roughness) depending on the DP of the PBzMA. A two-population SAXS model has been developed in order to characterize the globules protruding from the vesicle membrane. The mean globule diameter increases monotonically from 36 nm to 85 nm when the diblock copolymer precursor is chain-extended with 97-400 units of BzMA. Unlike the $G_{63}H_{350}$ diblock copolymer precursor vesicles, the *framboidal* triblock copolymer vesicles withstand high shear homogenization conditions and can therefore act as Pickering emulsifiers for the stabilization of *n*-dodecane droplets. Turbidimetry data support the literature hypothesis that greater surface roughness does indeed promote higher Pickering emulsifier efficiencies. More specifically, *framboidal* vesicles with mean globule dimensions of 45 nm exhibit aA_{eff} of up to 94%. PISA represents a highly convenient and versatile synthetic route to colloidal particles of exquisitely tunable surface roughness. Such nanoparticles may also be of interest for other fundamental scientific studies, such as the effect of surface topology on cell uptake kinetics.³⁶

Experimental

Materials and methods

Materials. All reagents were used as received unless otherwise stated. Benzyl methacrylate (BzMA), *n*-dodecane and 4, 4'-azobis-4-cyanopentanoic acid (ACVA) were purchased from Sigma-Aldrich (UK). BzMA inhibitor was removed by passing this monomer through an inhibitor removal column. Ethanol, dichloromethane, DMSO and DMF were purchased from Fisher Scientific (UK). Glycerol monomethacrylate (GMA) was kindly donated by GEO Specialty Chemicals (Hythe) and used without further purification. 2-Hydroxypropyl methacrylate (HPMA) was purchased from Alfa Aesar (UK) and contained 0.07 mol % dimethacrylate impurity, as judged by high performance liquid chromatography (HPLC). CD_3OD and d_6 -DMSO NMR solvents were purchased from Goss Scientific (UK). 4-Cyano-4-(2-phenylethanesulfanylthiocarbonyl)sulfanyl-pentanoic acid (PETTC) was synthesized in-house.³⁷ Deionized water was obtained using an Elga Elgastat Option 3A water purifier; its pH was approximately 6.2 and its surface tension was 72.0 mN m⁻¹ at 20 °C.

RAFT synthesis of PGMA macro-CTA agent in ethanol. A round-bottomed flask was charged with GMA (30.0 g; 187 mmol), PETTC (1.01 g; 2.97 mmol), ACVA (167 mg, 0.156 mmol) and ethanol (39.5 g). The sealed reaction vessel was purged with N₂ for 30 min and placed in a pre-heated oil bath at 70 °C for 135 min. The resulting PGMA macro-CTA (GMA conversion = 87 %; M_n = 17,600 g mol⁻¹, M_w/M_n = 1.16) was purified by precipitation into excess dichloromethane. A mean DP of 63 was calculated for this macro-CTA using ¹H NMR spectroscopy by comparison of the integral from 3.4 ppm to 4.3 ppm due to five protons from the PGMA with that of the peaks around 7 ppm due to the five aromatic protons from the RAFT CTA (see Figure S2).

Preparation of linear PGMA-HPMA diblock copolymer precursor vesicles via RAFT aqueous dispersion polymerization at 15 % w/w solids. PGMA₆₃ macro-CTA (5.00 g, 0.485 mmol), HPMA monomer (24.5 g, 170 mmol) and deionized water (167 g, purged with N₂ for 30 min) were weighed into a 250 mL round-bottomed flask and purged with N₂ for 20 min. ACVA was added (68.9 mg, 0.242 mmol, CTA/ACVA molar ratio = 2.0) and purged with N₂ for a further 10 min prior to immersion in an oil bath set at 70 °C for 2 h. Finally, the polymerization was quenched by cooling to room temperature with subsequent exposure to air.

Preparation of PGMA-HPMA-PBzMA triblock copolymer vesicles via RAFT seeded emulsion polymerization at 10-19 % w/w solids. PGMA₆₃-HPMA₃₅₀ diblock precursor vesicles (15.0 ml of a 10 % w/w copolymer dispersion, 1.50 g copolymer, 0.0247 mmol), ACVA (1.38 mg, 0.00494 mmol, CTA/ACVA molar ratio = 5.0) and BzMA monomer (0.109 g, 0.617 mmol, target DP = 25) were weighed into a 40 ml sample vial and purged with N₂ for 20 min prior to

immersion in an oil bath set at 70 °C for 4 h. Then the polymerization was quenched by cooling to room temperature and subsequent exposure to air. A series of similar copolymer syntheses were performed for which the PBzMA target DP ranged from 50 to 400 using BzMA masses varying from 0.218 g to 1.74 g (1.23 mmol to 9.87 mmol), respectively.

Pickering emulsion formation. *n*-Dodecane (2.0 ml) was homogenized with 2.0 ml of a 0.5–3.0 % w/v aqueous vesicle dispersion for 2 min using a IKA Ultra-Turrax T-18 homogenizer with a 10 mm dispersing tool operating at 12,000 rpm. The droplets were imaged by OM and the mean droplet diameter was assessed by laser diffraction.

Turbidimetry experiments. Pickering emulsions were allowed to cream overnight before an appropriate amount of the aqueous phase was extracted and diluted ten-fold, before measuring the absorbance from 400 to 800 nm using visible absorption spectroscopy. Calibration plots were constructed for each vesicle dispersion by recording the absorbance at 750 nm of the vesicle dispersions, varying the copolymer concentration from 0.00625 to 0.1 % w/w.

Characterization

¹H NMR spectroscopy. All NMR spectra were recorded using a 400 MHz Bruker Avance-400 spectrometer and 64 scans were averaged per spectrum. The mean DP of the PBzMA block was calculated as described previously by Chambon et al.²⁴

Gel permeation chromatography (GPC). Copolymer molecular weights and polydispersities were determined using a DMF GPC set-up operating at 60 °C and comprising two Polymer Laboratories PL gel 5 μm Mixed C columns connected in series to a Varian 390 LC multi-detector suite (only the refractive index detector was utilized) and a Varian 290 LC pump injection module. The GPC eluent was HPLC grade DMF containing 10 mM LiBr at a flow rate of 1.0 mL min⁻¹. DMSO was used as a flow-rate marker. Calibration was conducted using a series of ten near-monodisperse poly(methyl methacrylate) standards ($M_n = 625 - 618,000$ g mol⁻¹). The chromatograms were analyzed using Varian Cirrus GPC software (version 3.3) provided by the instrument manufacturer (Polymer Laboratories).

Dynamic light scattering (DLS). Intensity-average hydrodynamic diameters of the copolymer dispersions were determined using a Malvern Zetasizer NanoZS instrument. Dilute aqueous dispersions (0.10 % w/w) were analyzed using disposable cuvettes and all data were averaged over three consecutive runs to give the hydrodynamic diameter (D_h).

Transmission electron microscopy (TEM). Aggregate solutions were diluted fifty-fold at 20 °C to generate 0.10 % w/w dispersions. Copper/palladium TEM grids (Agar Scientific) were surface-coated in-house to yield a thin film of amorphous carbon. The grids were then plasma glow-discharged for 30 s to create a hydrophilic surface.

Individual samples (0.1 % w/w, 12 μL) were adsorbed onto the freshly glow-discharged grids for 1 min and then blotted with filter paper to remove excess solution. To stain the aggregates, uranyl formate (0.75 w/v %) solution (9 μL) was soaked on the sample-loaded grid for 20 s and then carefully blotted to remove excess stain. The grids were then dried using a vacuum hose. Imaging was performed on a Phillips CM100 instrument at 100 kV, equipped with a Gatan 1 K CCD camera.

Small-angle X-ray scattering (SAXS). SAXS patterns were recorded at two synchrotron sources (ESRF, station ID02, Grenoble, France and Diamond Light Source, station I22, Didcot, UK). A monochromatic X-ray radiation (wavelength $\lambda = 0.0995$ nm and 0.1001 nm, respectively) and 2D SAXS detectors (FReLoN Kodak CCD and Pilatus 2M, respectively) were used for these experiments. The SAXS camera length set-ups covered the q range from 0.009 nm⁻¹ to 0.04 nm⁻¹ (ESRF) and from 0.02 nm⁻¹ to 1.9 nm⁻¹ (Diamond), where $q = \frac{4\pi\sin\theta}{\lambda}$ is the modulus of the scattering vector and θ is one-half of the scattering angle. Either a 2.0 mm diameter glass capillary (ESRF) or a liquid cell composed of two mica windows (each of 25 μm thickness) separated by a polytetrafluoroethylene spacer of 1 mm thickness (Diamond) were used as sample holders, respectively. X-ray scattering data were reduced by Nika SAS data reduction macros for Igor Pro (integration, normalization, background subtraction) and were further analyzed using Irena SAS macros for Igor Pro. SAXS measurements were conducted on PGMA₆₃PHPMA₃₅₀PBzMA_z ($z = 0 - 400$, see Table S1) dispersions either in water (ESRF and Diamond) or in a 40 % w/w aqueous sucrose solution (Diamond). The copolymer concentration was diluted from 10 % w/w (as-synthesized) to 1.0 % w/w for data collection.

Visible absorption spectroscopy. Turbidities of both the initial vesicle dispersions and also the underlying aqueous phase of the corresponding creamed emulsions after homogenization with *n*-dodecane were assessed by visible absorption spectrophotometry (Perkin-Elmer Lambda 25 instrument) between 400 and 800 nm at a scan speed of 960 nm min⁻¹.

Optical microscopy (OM). Optical microscopy images were recorded using a Motic DMBA300 digital biological microscope with a built-in camera and equipped with Motic Images Plus 2.0 ML software.

Laser diffraction. A Malvern Mastersizer 2000 instrument equipped with a small volume Hydro 2000SM sample dispersion unit (ca. 50 ml), a He-Ne laser operating at 633 nm, and a solid-state blue laser operating at 466 nm was used to size each emulsion. The stirring rate was adjusted to 1,000 rpm in order to avoid creaming of the emulsion during analysis. After each measurement, the cell was rinsed once with ethanol, followed by three rinses with doubly-distilled water; the glass walls of the cell were carefully wiped with lens cleaning tissue to avoid cross-

contamination and the laser was aligned centrally to the detector prior to data acquisition. The volume-average diameter was measured and repeated four times for each emulsion.

Acknowledgements

Christopher Hill and Svetomir Tzokov at the University of Sheffield Biomedical Science Electron Microscopy Suite. The authors are grateful to ESRF (France) and Diamond (U.K.) for providing SAXS beamtime. Diego Pontoni (PSCM) and the personnel of ID02 station are thanked for help with SAXS experiments. Dr. Andrew J. Morse is thanked for SEM images. SPA thanks the European Research Council for an ERC Advanced Investigator grant (PISA 320372) to support CJM, OOM, NJW and KLT and also EPSRC for a Platform grant (EP/J007846/1) to support OOM, KLT and NJW.

References

- S. U. Pickering, *Journal of the Chemical Society*, 1907, **91**, 2001-2021.
- B. P. Binks, *Current Opinion in Colloid & Interface Science*, 2002, **7**, 21-41.
- Z. Mao, H. Xu and D. Wang, *Advanced Functional Materials*, 2010, **20**, 1053-1074.
- B. P. Binks and S. O. Lumsdon, *Physical Chemistry Chemical Physics*, 1999, **1**, 3007-3016.
- S. Levine, B. D. Bowen and S. J. Partridge, *Colloids and Surfaces*, 1989, **38**, 325-343.
- B. P. Binks and S. O. Lumsdon, *Langmuir*, 2001, **17**, 4540-4547.
- K. L. Thompson, S. P. Armes, J. R. Howse, S. Ebbens, I. Ahmad, J. H. Zaidi, D. W. York and J. A. Burdis, *Macromolecules*, 2010, **43**, 10466-10474.
- K. L. Thompson, S. P. Armes, D. W. York and J. A. Burdis, *Macromolecules*, 2010, **43**, 2169-2177.
- A. Walsh, K. L. Thompson, S. P. Armes and D. W. York, *Langmuir*, 2010, **26**, 18039-18048.
- Y. Cui, M. Threlfall and J. S. van Duijneveldt, *Journal of Colloid and Interface Science*, 2011, **356**, 665-671.
- J. Chiefari, Y. K. Chong, F. Ercole, J. Krstina, J. Jeffery, T. P. T. Le, R. T. A. Mayadunne, G. F. Meijs, C. L. Moad, G. Moad, E. Rizzardo and S. H. Thang, *Macromolecules*, 1998, **31**, 5559-5562.
- W. Zhang, F. D'Agosto, P.-Y. Dugas, J. Rieger and B. Charleux, *Polymer*, 2013, **54**, 2011-2019.
- K. L. Thompson, P. Chambon, R. Verber and S. P. Armes, *Journal of the American Chemical Society*, 2012, **134**, 12450-12453.
- Z. Wang, M. C. M. van Oers, F. P. J. T. Rutjes and J. C. M. van Hest, *Angewandte Chemie International Edition*, 2012, **51**, 10746-10750.
- A. San-Miguel and S. H. Behrens, *Langmuir*, 2012, **28**, 12038-12043.
- R. Van Hooghten, L. Imperiali, V. Boeckx, R. Sharma and J. Vermant, *Soft Matter*, 2013, **9**, 10791-10798.
- Y. Li and S. P. Armes, *Angewandte Chemie International Edition*, 2010, **49**, 4042-4046.
- B. Charleux, G. Delaître, J. Rieger and F. D'Agosto, *Macromolecules*, 2012, **45**, 6753-6765.
- Z. An, Q. Shi, W. Tang, C.-K. Tsung, C. J. Hawker and G. D. Stucky, *Journal of the American Chemical Society*, 2007, **129**, 14493-14499.
- G. Delaître, M. Save and B. Charleux, *Macromolecular Rapid Communications*, 2007, **28**, 1528-1533.
- J. Rieger, C. Gazon, B. Charleux, D. Alaimo and C. Jérôme, *Journal of Polymer Science Part A: Polymer Chemistry*, 2009, **47**, 2373-2390.
- A. Blanazs, A. J. Ryan and S. P. Armes, *Macromolecules*, 2012, **45**, 5099-5107.
- A. Blanazs, J. Madsen, G. Battaglia, A. J. Ryan and S. P. Armes, *Journal of the American Chemical Society*, 2011, **133**, 16581-16587.
- P. Chambon, A. Blanazs, G. Battaglia and S. P. Armes, *Macromolecules*, 2012, **45**, 5081-5090.
- L. Houillot, C. Bui, M. Save, B. Charleux, C. Farcet, C. Moire, J.-A. Raust and I. Rodriguez, *Macromolecules*, 2007, **40**, 6500-6509.
- J. A. Balmer, O. O. Mykhaylyk, A. Schmid, S. P. Armes, J. P. A. Fairclough and A. J. Ryan, *Langmuir*, 2011, **27**, 8075-8089.
- J. A. Balmer, O. O. Mykhaylyk, J. P. A. Fairclough, A. J. Ryan, S. P. Armes, M. W. Murray, K. A. Murray and N. S. J. Williams, *Journal of the American Chemical Society*, 2010, **132**, 2166-2168.
- L. A. Fielding, O. O. Mykhaylyk, S. P. Armes, P. W. Fowler, V. Mittal and S. Fitzpatrick, *Langmuir*, 2012, **28**, 2536-2544.
- L. A. Fielding, O. O. Mykhaylyk, A. Schmid, D. Pontoni, S. P. Armes and P. W. Fowler, *Chemistry of Materials*, 2014, **26**, 1270-1277.
- L. J. Fetters, D. J. Lohse and R. H. Colby, in *Physical Properties of Polymers Handbook*, ed. J. Mark, Springer New York, 2007, pp. 447-454.
- N. J. Warren, O. O. Mykhaylyk, A. J. Ryan, M. Williams, T. Doussineau, P. Dugourd, R. Antoine, G. Portale and S. P. Armes, *Journal of the American Chemical Society*, 2015, **137**, 1929-1937.
- N. J. Warren, O. O. Mykhaylyk, A. J. Ryan, M. Williams, T. Doussineau, P. Dugourd, R. Antoine, G. Portale and S. P. Armes, *Journal of the American Chemical Society*, 2014.
- K. L. Thompson, C. J. Mable, A. Cockram, N. J. Warren, V. J. Cunningham, E. R. Jones, R. Verber and S. P. Armes, *Soft Matter*, 2014, **10**, 8615-8626.
- R. N. Wenzel, *Industrial & Engineering Chemistry*, 1936, **28**, 988-994.
- A. B. D. Cassie and S. Baxter, *Transactions of the Faraday Society*, 1944, **40**, 546-551.
- I. Canton and G. Battaglia, *Chemical Society Reviews*, 2012, **41**, 2718-2739.
- E. R. Jones, M. Semsarilar, A. Blanazs and S. P. Armes, *Macromolecules*, 2012, **45**, 5091-5098.

